arXiv:1701.06769v1 [cond-mat.mes-hall] 24 Jan 2017

Density of states of Dirac-Landau levels in a gapped graphene monolayer under strain gradient

V O Shubnyi[1] and S G Sharapov[2]

[1] Department of Physics, Taras Shevchenko National Kiev University, 6 Academician Glushkov ave., Kiev 03680, Ukraine
[2] Bogolyubov Institute for Theoretical Physics, National Academy of Science of Ukraine, 14-b Metrolohichna Street, Kiev 03680, Ukraine

E-mail: sharapov@bitp.kiev.ua

Abstract. We study a gapped graphene monolayer in a combination of uniform magnetic field and strain-induced uniform pseudomagnetic field. The presence of two fields completely removes the valley degeneracy. The resulting density of states shows a complicated behaviour that can be tuned by adjusting the strength of the fields. We analyze how these features can be observed in the sublattice, valley and full density of states. The analytical expression for the valley DOS is derived.

Submitted to: *J. Phys.: Condens. Matter*

1. Introduction

The carbon atoms in monolayer graphene form a honeycomb lattice due to sp^2 hybridisation of their orbitals. Since the honeycomb lattice is not a Bravais lattice, one has to consider the honeycomb lattice as a triangular Bravais lattice with two atoms per until cell. Thus one naturally arrives at a two-component spinor wave function of the quasiparticle excitations in graphene (see Ref. [1] for some analogies with a real spin). These components reflect the amplitude of the electron wave function on the A and B sublattices. The two-component form of the wave function along with the band structure results in the Dirac form of the effective theory for graphene.

The Dirac fermions had shown up the celebrated magneto-transport and STS properties of graphene (see Refs. [2, 3, 4] for the reviews). Recently STM/STS measurements allowed not only to observe relativistic Landau levels, but also to resolve directly their sublattice specific features. By resolving density of states (DOS) on A and B sublattices of a gapped graphene, it was experimentally confirmed [5] that the amplitude of the wave function of the lowest Landau level (LLL) is unequally distributed between the sublattices depending on its energy sign.

In the presence of a gap Δ driven by inversion symmetry breaking, the LLL splits into two levels with the energy $E_0 = \eta\Delta\mathrm{sgn}\,(eB)$, where $\eta = \pm$ distinguishes inequivalent $\mathbf{K}$ and $\mathbf{K}'$ points of the Brillouin zone and an external magnetic field $\mathbf{B} = \nabla \times \mathbf{A} = (0, 0, B)$ is applied perpendicularly to the plane of graphene along

the positive z axis [6]. Here $e = -|e|$ is the electron charge and $\mathbf{A}$ is the vector electromagnetic potential. The corresponding amplitudes of the wave function of the positive energy electron-like, 0_+, and negative energy hole-like, 0_-, levels are on A and B sublattices. In other words, the individual sublattices are valley polarized for the LLL [7].

An exciting opportunity for manipulating the amplitudes of the wave function on the sublattices opens due to close connection between the impact of deformation and external electromagnetic field on the electron structure of graphene. Change in hopping energy between A and B atoms induced by strain can be described by vector potential $\mathbf{A}_{\rm pm}$ analogous to the vector potential $\mathbf{A}$ of the external magnetic field (see Refs. [8, 9] for a review).

The corresponding field, $\mathbf{B}_{\rm pm} = \nabla \times \mathbf{A}_{\rm pm}$, is called pseudomagnetic field (PMF), because it is directed oppositely in $\mathbf{K}$ and $\mathbf{K}'$ valleys. This implies that the LLL breaks the electron-hole symmetry, with the LLL energy, $E_0 = \Delta \mathrm{sgn}\,(B_{\rm pm})$ for both $\mathbf{K}$ and $\mathbf{K}'$ points. Furthermore, the states corresponding to the LLL are sublattice polarized, because they reside exclusively on either A or B sublattice [7].

While the formation of the LLL is associated with zero modes and does not require a homogeneous PMF, to form higher Landau levels a uniform PMF is needed [10]. This is in fact the main challenge [11] for the implementation of strained graphene, although recently there has been some progress both in experiment [12, 13, 14] and in theory [15].

In the presence of either external magnetic field or deformation, the higher energy levels from $\mathbf{K}$ and $\mathbf{K}'$ points remain degenerate. This degeneracy is lifted when both strain and magnetic field are present. One of the interesting consequences of the lifting is that for $|B_{\rm pm}| > |eB|$, the Hall conductivity is oscillating between 0 and $\mp 2e^2/h$ [16].

The latest experiments [14] show that it is possible to create a homogeneous PMF of order of a few Tesla. Therefore, there is a good chance that the STS/STM measurements of the Dirac Landau levels similar to that done in Ref. [5] are now possible on strained graphene. Thus the purpose of the present work is to study the DOS (including the sublattice resolved) in a combination of a constant PMF $B_{\rm pm}$ created by non-uniform strain and magnetic field B. In particular, we will look for the specific effects related to the presence of nonzero gap Δ and lifting of the degeneracy between $\mathbf{K}$ and $\mathbf{K}'$ that can be observed in STS measurements.

The paper is organized as follows. We begin by presenting in section 2 the model describing gapped monolayer graphene in the combination of PMF and magnetic field. In section 3 we provide the definitions of the valley, sublattice and full DOS in terms of the Green's function decomposed over Landau levels. The corresponding DOS are written in section 4 as the sums that in the case of the valley DOS can be calculated analytically. The results for the DOS in the various regimes are discussed in section 5 and conclusions are given in section 6.

2. Model

We consider gapped monolayer graphene in the continuum approximation described by the effective Hamiltonian

$$H = \begin{pmatrix} H_{\mathbf{K}} & 0 \\ 0 & H_{\mathbf{K}'} \end{pmatrix}, \tag{1}$$

The full Hamiltonian (1) acts on wave function with four components

$$\Psi = \begin{pmatrix} \psi^{\bullet}_{\mathbf{K}} \\ \psi^{\circ}_{\mathbf{K}} \\ \psi^{\circ}_{\mathbf{K}'} \\ \psi^{\bullet}_{\mathbf{K}'} \end{pmatrix}, \tag{2}$$

where $\bullet$ and $\circ$ denote, respectively, A and B sublattices and we followed the notations of Refs. [6, 3] with exchanging the sublattices in the $\mathbf{K}'$ valley. Thus the Hamiltonian (1) includes two blocks corresponding to $\mathbf{K}$ and $\mathbf{K}'$ valleys

$$H_{\mathbf{K}} = v_F \boldsymbol{\tau} \left(-i\hbar\nabla - \frac{e}{c}\mathbf{A} - \mathbf{A}_{\rm pm} \right) + \tau_3 \Delta, \tag{3}$$

$$H_{\mathbf{K}'} = -v_F \boldsymbol{\tau} \left(-i\hbar\nabla - \frac{e}{c}\mathbf{A} + \mathbf{A}_{\rm pm} \right) - \tau_3 \Delta. \tag{4}$$

Here $\boldsymbol{\tau} = (\tau_1, \tau_2)$ and τ_3 are Pauli matrices acting in the sublattice space, v_F is the Fermi velocity, the gap Δ corresponds to the energy difference 2Δ between the A and B sublattices, $\mathbf{A}$ and $\mathbf{A}_{\rm pm}$ are the the electromagnetic and strain induced vector potentials, respectively. We neglect the spin splitting, because for commonly used strengths of magnetic field the Zeeman splitting is small compared to the distance between the Landau levels. For a fixed direction of external magnetic field, the corresponding to $\mathbf{A}$ term in the Hamiltonian breaks time-reversal symmetry, while the $\mathbf{A}_{\rm pm}$ term breaks the inversion symmetry and leaves time-reversal symmetry unbroken.

With the x-axis aligned in the zigzag direction, the strain-induced vector potential reads [17, 18] (see also the reviews [8, 9])

$$\mathbf{A}_{\rm pm} = \frac{\hbar\beta\kappa}{2a_0} \begin{pmatrix} u_{xx} - u_{yy} \\ -2u_{xy} \end{pmatrix}, \tag{5}$$

where $\beta = -\partial \ln t / \partial \ln a|_{a=a_0} \approx 3$ is the dimensionless electron Grüneisen parameter for the lattice deformation, t the nearest-neighbour hopping parameter, $\kappa \approx 1/3$ is a parameter related to graphene's elastic property [17], a is the length of the carbon-carbon bond, (a_0 is the length of the unstrained bond), and u_{ij} with $i, j = x, y$ is the strain tensor as defined in classical continuum mechanics [8, 9]. We also assume that the deformation is a pure shear, so that $u_{xx} + u_{yy} = 0$, and there is no scalar potential term in the Hamiltonian.

The sign of the PMF depends on the valley, and, for example, in $\mathbf{K}$ valley,

$$B_{\rm pm} = -\frac{\hbar\beta\kappa}{a_0} \left(\partial_x u_{xy} + \frac{1}{2}\partial_y (u_{xx} - u_{yy}) \right), \tag{6}$$

whereas it has the opposite sign in $\mathbf{K}'$ valley, because $\mathbf{A}_{\rm pm}$ enters Eqs. (3) and (4) with the opposite signs. Eq. (6) illustrates the main problem in this field of research, viz. a uniform PMF can only be created by a non-uniform strain [11]. As was already stated in the Introduction, considering the experimental progress achieved in the field [14], we restrict ourselves to a constant PMF. Thus we arrive at the model with two independent $\mathbf{K}$ points characterized by the following combinations of the fields, $B_{\pm} = eB/c \pm B_{\rm pm}$. A more complicated, but analytically intractable case with a combination of a constant magnetic and inhomogeneous pseudomagnetic fields was considered in Ref. [19], where a circularly symmetric strain is induced by a homogeneous load.

3. Green's function, sublattice and valley resolved DOS

Although it is straightforward to obtain the DOS directly from the solution of the corresponding Dirac equation, we rely on the Green's function (GF) machinery that automatically takes into account the degeneracy of levels and avoids the necessity to work with different directions of fields separately. Since the **K** points in the model (1) are independent, we will use the GF's corresponding to the separate **K** points. In particular, we are interested in the translation invariant part $\widetilde{G}$ of the GF that allows to derive both the DOS and the transport coefficients. Its derivation using the Schwinger proper-time method and decomposition over Landau-level poles has been discussed in many papers (see, e.g., Refs. [20, 21, 22, 23]). Here we begin with the translation invariant part for **K** point written in the Matsubara representation (we set $\hbar = c = k_B = 1$ in what follows)

$$\widetilde{G}^{\mathbf{K}}(\mathrm{i}\omega, \mathbf{p}) = \mathrm{e}^{-\frac{p^2}{|B_+|}} \sum_{n=0}^{\infty} (-1)^n \frac{G_n(B_+, \mathrm{i}\omega, \mathbf{p})}{(\mathrm{i}\omega)^2 - (M_n^+)^2}, \qquad \omega = \pi(2m+1)T, \tag{7}$$

where T is the temperature,

$$M_n^{\pm} = \sqrt{\Delta^2 + 2nv_F^2|B_{\pm}|} \tag{8}$$

are the energies of the relativistic Landau levels at **K** and **K**′ points ($\eta = \pm$), respectively, and the function

$$\begin{aligned} G_n(B_+, \mathrm{i}\omega, \vec{p}) = (\Delta\,\tau_3 + \mathrm{i}\omega) \Bigg[& (1 + \tau_3\,\mathrm{sgn}(B_+)) L_n\left(\frac{2p^2}{|B_+|}\right) \\ & - (1 - \tau_3\,\mathrm{sgn}(B_+)) L_{n-1}\left(\frac{2p^2}{|B_+|}\right)\Bigg] \\ & - 4v_F(p_x\tau_y + p_y\tau_x) L_{n-1}^1\left(\frac{2p^2}{|B_+|}\right). \end{aligned} \tag{9}$$

Here $L_n^{\alpha}(z)$ are the generalized Laguerre polynomials, and $L_n(z) \equiv L_n^0(z)$ ($L_{-1}^1 \equiv 0$). When deriving GF from the known wave-functions, the Laguerre polynomials originate from the integration of two Hermite polynomials with proper weights. Looking at the structure of the GF (7), one can see that the projectors $P_{\pm} = (1 \pm \tau_3\mathrm{sgn}(B_+))/2$ take into account that, for example, for $B_+ > 0$, the states on A and B sublattices involve L_n and L_{n-1}, respectively. The most general expression of the propagator in the presence of B, B_{pm} and various types of the gaps is provided in [24].

The corresponding contribution of the **K** point to the DOS per spin and unit area on A and B sublattices reads

$$D_{A,B}^{\mathbf{K}}(\epsilon) = \frac{1}{2\pi i} \int \frac{d^2p}{(2\pi)^2} [\widetilde{G}_{ii}^{\mathbf{K}}(\epsilon - i0, \mathbf{p}) - \widetilde{G}_{ii}^{\mathbf{K}}(\epsilon + i0, \mathbf{p})] \tag{10}$$

with $i = 1, 2$ for A and B sublattices. It follows from Eq. (1) that

$$\widetilde{G}^{\mathbf{K}'}(\mathrm{i}\omega, \mathbf{p}) = \widetilde{G}^{\mathbf{K}}(v_F \to -v_F, \Delta \to -\Delta, B_+ \to B_-) \tag{11}$$

and

$$D_{B,A}^{\mathbf{K}'}(\epsilon) = \frac{1}{2\pi i} \int \frac{d^2p}{(2\pi)^2} [\widetilde{G}_{ii}^{\mathbf{K}'}(\epsilon - i0, \mathbf{p}) - \widetilde{G}_{ii}^{\mathbf{K}'}(\epsilon + i0, \mathbf{p})] \tag{12}$$

with $i = 1, 2$ for B and A sublattices, i.e. exchanging the sublattices. While the valley resolved DOS presents a theoretical interest and will also be considered below,

the STS measurements allow to observe the full DOS involving two valleys on each sublattice

$$D_{A,B}(\epsilon) = D^{\mathbf{K}}_{A,B}(\epsilon) + D^{\mathbf{K}'}_{A,B}(\epsilon). \tag{13}$$

We will also consider the valley resolved but summed over sublattices DOS

$$D^{\mathbf{K},\mathbf{K}'}(\epsilon) = D^{\mathbf{K},\mathbf{K}'}_{A}(\epsilon) + D^{\mathbf{K},\mathbf{K}'}_{B}(\epsilon) \tag{14}$$

which presents interest for valleytronics. Finally, the full DOS can also be found by summing the valley resolved DOS

$$D(\epsilon) = D^{\mathbf{K}}(\epsilon) + D^{\mathbf{K}'}(\epsilon). \tag{15}$$

4. Expressions for numerical and analytical calculation of the DOS

Using the integral [25]

$$\int \frac{\mathrm{d}^2 p}{(2\pi)^2} L_n\left(\frac{2p^2}{|B|}\right) \exp\left(-\frac{p^2}{|B|}\right) = \frac{(-1)^n}{2\pi}\frac{|B|}{2} \tag{16}$$

and evaluating the discontinuity of the GF we arrive at the final result

$$D^{\mathbf{K},\mathbf{K}'}_{A,B}(\epsilon) = D^{\mathbf{K},\mathbf{K}'(0)}_{A,B}(\epsilon) + D^{\mathbf{K},\mathbf{K}'(n\geq 1)}_{A,B}(\epsilon). \tag{17}$$

Here $D^{\mathbf{K},\mathbf{K}'(0)}_{A,B}(\epsilon)$ is the LLL contribution to the valley and sublattice resolved DOS and $D^{\mathbf{K},\mathbf{K}'(n\geq 1)}_{A,B}(\epsilon)$ is the corresponding contribution from the Landau levels with $n \geq 1$. Explicit expressions for these terms are

$$D^{\mathbf{K}(0)}_{A}(\epsilon) = \frac{|B_+|}{2\pi}\theta(B_+)\delta(\epsilon-\Delta), \qquad D^{\mathbf{K}'(0)}_{A}(\epsilon) = \frac{|B_-|}{2\pi}\theta(-B_-)\delta(\epsilon-\Delta), \tag{18}$$

$$D^{\mathbf{K}(0)}_{B}(\epsilon) = \frac{|B_+|}{2\pi}\theta(-B_+)\delta(\epsilon+\Delta), \qquad D^{\mathbf{K}'(0)}_{B}(\epsilon) = \frac{|B_-|}{2\pi}\theta(B_-)\delta(\epsilon+\Delta), \tag{19}$$

and for the Landau levels with $n \geq 1$,

$$D^{\mathbf{K},\mathbf{K}'(n\geq 1)}_{A}(\epsilon) = \sum_{n=1}^{\infty} \frac{|B_\pm|}{2\pi}\left[\frac{M^\pm_n+\Delta}{2M^\pm_n}\delta(\epsilon-M^\pm_n) + \frac{M^\pm_n-\Delta}{2M^\pm_n}\delta(\epsilon+M^\pm_n)\right], \tag{20}$$

$$D^{\mathbf{K},\mathbf{K}'(n\geq 1)}_{B}(\epsilon) = \sum_{n=1}^{\infty} \frac{|B_\pm|}{2\pi}\left[\frac{M^\pm_n-\Delta}{2M^\pm_n}\delta(\epsilon-M^\pm_n) + \frac{M^\pm_n+\Delta}{2M^\pm_n}\delta(\epsilon+M^\pm_n)\right], \tag{21}$$

where $\pm$ sign corresponds to $\mathbf{K}$ and $\mathbf{K}'$ points. As expected, presence of PMF removes degeneracy of the levels with $n \geq 1$ [16] .

In section 5 we compute the sublattice and valley resolved DOS numerically on the base of Eqs. (18), (19), (20) and (21) by widening δ-fuction peaks to a Lorentzian shape, viz.

$$\delta(\epsilon - M_n) \to \frac{1}{\pi}\frac{1}{(\epsilon-M_n)^2+\Gamma_n^2}, \tag{22}$$

where Γ_n is the n-th level width. Such broadening of Landau levels with a constant Γ was found to be rather a good approximation valid in not very strong magnetic fields.

4.1. The DOS in the zero pseudomagnetic field

Setting $B_{\rm pm} = 0$ we recover the well-known results that were experimentally observed in [5]. Then Eqs. (18) and (19) result in the sublattice DOS

$$D_A^{(0)}(\epsilon) = \frac{|eB|}{2\pi}\delta(\epsilon - \Delta), \qquad D_B^{(0)}(\epsilon) = \frac{|eB|}{2\pi}\delta(\epsilon + \Delta). \tag{23}$$

This confirms that the LLL is valley polarized, because each LLL contribution to the DOS comes from either $\mathbf{K}$ or $\mathbf{K}'$ valley, as discussed in the Introduction. This feature has to be contrasted with the valley resolved but summed over the two sublattices DOS

$$D^{\mathbf{K},\mathbf{K}'(0)}(\epsilon) = D_A^{\mathbf{K},\mathbf{K}'(0)}(\epsilon) + D_B^{\mathbf{K},\mathbf{K}'(0)}(\epsilon) = \frac{|eB|}{2\pi}\delta(\epsilon - \eta\Delta\mathrm{sgn}\,(eB)). \tag{24}$$

For $n \geq 1$ the levels at $\mathbf{K}$ and $\mathbf{K}'$ points described by Eqs. (20) and (21) are degenerate, but the DOS on A and B sublattices differs and this effect is observable [5].

4.2. The DOS in the zero magnetic field

Setting $eB = 0$ we obtain from Eqs. (18) and (19) that the LLL contribution to the sublattice DOS is

$$D_A^{(0)}(\epsilon) = \frac{|B_{\rm pm}|}{2\pi}\theta(B_{\rm pm})\delta(\epsilon - \Delta), \qquad D_B^{(0)}(\epsilon) = \frac{|B_{\rm pm}|}{2\pi}\theta(-B_{\rm pm})\delta(\epsilon + \Delta) \tag{25}$$

This confirms that the LLL is sublattice polarized, as discussed in the Introduction.

4.3. Analytical expression for the valley DOS

Although the expressions for the sublattice and valley DOS presented in Sec. 3 are sufficient for the numerical study presented in Sec. 5, it is always useful to have a simple analytical expression for the DOS. One can notice that the the valley DOS, Eq. (14) is the sum of delta-functions (or Lorentzians when the the level widening is taken into account), because the sum of the weight factors $(M_n^{\pm} \pm \Delta)/(2M_n^{\pm})$ present in Eqs. (20) and (21) gives 1. This allows one to use the results of Ref. [26], and calculate the sum over Landau levels analytically

$$D^{\mathbf{K},\mathbf{K}'}(\epsilon) = \frac{1}{2\pi^2}\Bigg\{-|B_{\pm}|\theta(\mp B_{\pm})\frac{\Gamma}{(\epsilon-\Delta)^2+\Gamma^2} - |B_{\pm}|\theta(\pm B_{\pm})\frac{\Gamma}{(\epsilon+\Delta)^2+\Gamma^2} + \Gamma\ln\frac{\Lambda^2}{2|B_{\pm}|} - \mathrm{Im}\left[(\epsilon+\mathrm{i}\Gamma)\psi\left(\frac{\Delta^2-(\epsilon+\mathrm{i}\Gamma)^2}{2|B_{\pm}|}\right)\right]\Bigg\}. \tag{26}$$

Here ψ is the digamma function, $\pm$ sign corresponds to $\mathbf{K}$ and $\mathbf{K}'$ points, the width of all levels Γ is assumed to be the same, and Λ is the cutoff energy that has the order of bandwidth. Eq. (26) differs from Eq. (4.15) of Ref. [26] by the first two terms. In the present case they take care of the electron hole asymmetry of the LLL, while in [26] both $\mathbf{K}$ and $\mathbf{K}'$ points contribute to the full DOS. The advantage of Eq. (26) is that it allows to consider the low field regime when the direct numerical summation over many Landau levels is consuming.

5. Results

Now we use Eqs. (18), (19), (20) and (21) to study the valley (14), sublattice (13) and the full (15) DOS numerically. For simplicity we assume that all Landau levels have the same width Γ. In this case the valley DOS and then the full DOS can also be calculated using Eq. (26). To fit real experimental data [27] it may be necessary to consider the width, Γ_n, dependent on the Landau level index. This can be easily done in the framework of numerical computation of the sum over Landau levels. However, when all levels have the same width and one is interested in the valley DOS, it is more efficient to compute it from the analytical expression (26) which is easier to use in the low field regime. In all numerical work we take the value of the Fermi velocity, $v_F = 10^6$ m/s that corresponds to the Landau energy scale, $\epsilon_0 = (\hbar v_F^2 B_\pm)^{1/2} = 25.7\sqrt{B_\pm[\mathrm{T}]}$ meV. The gap Δ that lifts the energy degeneracy of the A and B sublattices and breaks the inversion symmetry was observed for a graphene monolayer on top of SiC, graphite [4], and hexagonal boron nitride [28]. Its value ranges from 10 meV to several tens of meV.

Fig. 1 demonstrates how the full density of states, Eq. (15), is formed by the contributions from the valley resolved DOS, Eq. (14): left panel (a) is for $|eB| < |B_{\mathrm{pm}}|$ and the right panel (b) is for $|eB| > |B_{\mathrm{pm}}|$. The two curves (thin solid red and

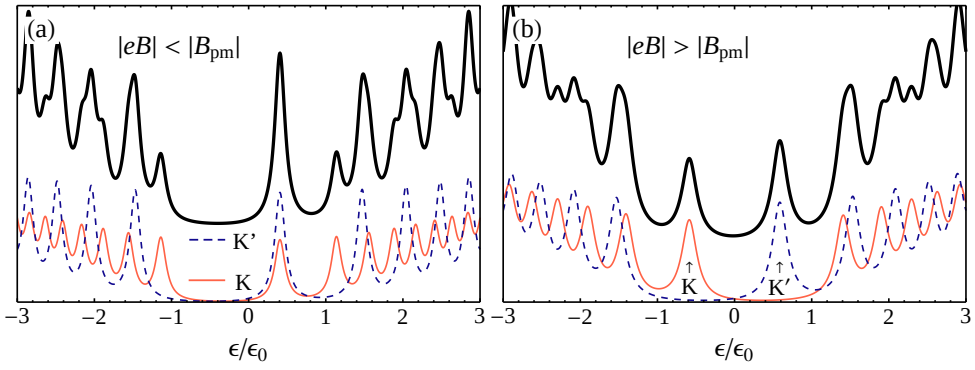

Figure 1. (Colour online) The full DOS, $D(\epsilon)$, (thick solid) and the valley-resolved DOS, $D^{\mathbf{K},\mathbf{K}'}(\epsilon)$, (thin solid and thin dashed) in arbitrary units as the functions of energy ϵ/ϵ_0, where $\epsilon_0 = (\hbar v_F^2 B_+)^{1/2} = 25.7\sqrt{B_+[\mathrm{T}]}$ meV is the Landau scale for $\mathbf{K}$ valley. Left panel: (a): the fields $B = 5$ T and $B_{\mathrm{pm}} = 18$ T. Right panel: (b): the fields $B = 10$ T and $B_{\mathrm{pm}} = 1$ T. The gap $\Delta = 50$ meV and the scattering rate $\Gamma = 10$ meV in the both cases.

thin dashed blue) in the bottom part of the figure show the valley resolved DOS, $D^{\mathbf{K},\mathbf{K}'}(\epsilon)$. The curves for $\mathbf{K}$ and $\mathbf{K}'$ points have the peaks corresponding to the relativistic Landau levels with the energies $\sim \pm\sqrt{n|B_\pm|}$. The position of the peaks corresponding the LLL with $E_0 = \pm\Delta$ distinguish the cases (a) the PMF dominated regime, $|eB| < |B_{\mathrm{pm}}|$, when both peaks have the same sign of the energy, and (b)

the magnetic field dominated regime, $|eB| > |B_{\rm pm}|$, when the peaks have the opposite energy sign. We checked that the same curves also follow from the analytical expression (26). Those are rather trivial consequences of having a superposition of magnetic and PMF.

The full DOS $D(\epsilon)$ shown by thick black curve in the two panels obviously has two series of peaks. One could see that in the special cases, the difference between two curves is substantial, and resulting DOS curve has irregular features and/or masked peaks. Depending on the values of the effective fields $B_\pm$, the Landau levels could be viewed as a splitting of one level (in case $|B_+| \approx |B_-|$) or as the two largely independent series, as for the case shown in Fig. 1.

Let us look closer at the pattern that overlapping Landau levels may create for certain values of B and $B_{\rm pm}$. The energies of the Landau levels with indices n_+, n_- for $\mathbf{K}$ and $\mathbf{K}'$ points coincide, viz. $M_{n_+} = M_{n_-}$ if there exist some values of B_+ and B_- satisfying the condition, $|B_+|n_+ = |B_-|n_-$. This implies that the fraction $|B_+|/|B_-| = a/b$ has to be rational. In terms of the initial fields B and $B_{\rm pm}$ this condition implies that

$$eB = \frac{1 - a/b}{1 + a/b} B_{\rm pm}. \tag{27}$$

The corresponding beating patterns for four values of the fraction a/b are shown in Fig. 2. The lowest (green) curve is for the simplest case, $B_-/B_+ = 1/2$. Each second

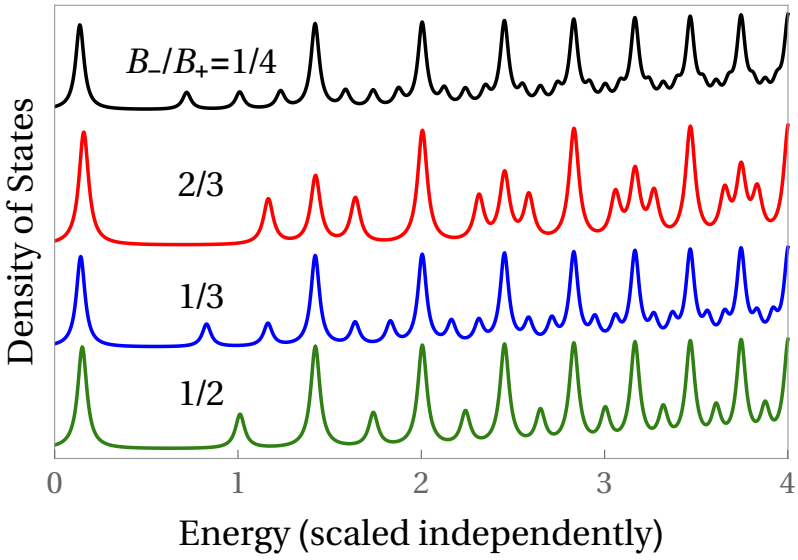

Figure 2. (Colour online) The full DOS, $D(\epsilon)$, in arbitrary units as the functions of energy ϵ/ϵ_0, where $\epsilon_0 = (\hbar v_F^2 B_+)^{1/2} = 25.7\sqrt{B_+[\mathrm{T}]}$ meV. The green curve is for $B_-/B_+ = 1/2$, the blue curve is for $B_-/B_+ = 1/3$, the red curve is for $B_-/B_+ = 2/3$ and the black curve is for $B_-/B_+ = 1/4$. The gap $\Delta = 10$ meV and the scattering rate $\Gamma = 2$ meV.

level with coinciding energies is enhanced. The second from the bottom (blue) curve is for $B_-/B_+ = 1/3$. In this case an enhancement occurs for each third level. The third from the bottom (red) curve is for $B_-/B_+ = 2/3$ has even more tricky pattern

with the highest each third level and each forth level of an intermediate height. The curve on the top (black) is for $B_-/B_+ = 1/4$.

It is instructive to represent the dependences of the full DOS, $D(\epsilon)$, on the fields B and $B_{\rm pm}$ employing the density plot. Since a wide range of the fields is involved, its consideration in the low field regime may demand summation over many Landau levels. Thus we use Eq. (26), where the summation is done analytically. Figs. 3 (a) and (b) on the top panel show the full DOS, $D(\epsilon, B, B_{\rm pm})$ as a function of energy ϵ in meV and magnetic field B in T for $B_{\rm pm} = 0$ T and $B_{\rm pm} = 8$ T. Figs. 3 (c) and (d) in the bottom panel show the full DOS, $D(\epsilon, B, B_{\rm pm})$ as a function of energy ϵ in meV and PMF $B_{\rm pm}$ in T for $B = 0$ T and $B = 8$ T. The density plot is partly overlaid with the solid (red) and dashed (blue) curves that show position of the peaks in the DOS originating from the Landau levels at $\mathbf{K}$ and $\mathbf{K}'$ points, respectively. Fig. 3 (a) (top left panel) describes unstrained graphene. The Landau levels fan away from the Dirac point at $\epsilon = 0$. One can find a similar DOS map for the STS measurements [4] of graphene on chlorinated SiO_2. In the real case the spectra are distorted at low fields due to the substrate induced disorder and are strongly position dependent. The density plot [4] allows to observe at higher fields the sequence of broadened Landau levels with separated peaks. Fig. 3 (c) (bottom left panel) describes strained graphene in zero magnetic field. It is almost identical to Fig. 3 (a) except to the LLL that in the case of strained graphene breaks the electron-hole symmetry. Fig. 3 (b) and (d) (right top and bottom panels) describe strained graphene in the external magnetic field. This case was also studied experimentally in [13], where SMT and STS measurements were made on the deformed by gating graphene drumhead.

Comparing all these panels we observe that in the presence of both PMF and magnetic field there exist regions of intersecting Landau levels with the opposite slope that are related to the opposite valleys. In Fig. 3 (b) this is the region with $|eB| < |B_{\rm pm}|$, while Fig. 3 (d) the corresponding region is seen for $|B_{\rm pm}| < |eB|$. This behaviour of Landau levels is almost obvious in the presented case. However, in the case of poorly resolved Landau levels this feature can be rather helpful for proving the presence of both PMF and magnetic field.

Finally, we illustrate in Fig. 4 how the full DOS is distributed between the sublattices. The DOS on A and B sublattices, $D_{A,B}(\epsilon)$, are shown by (dashed) green and solid (orange) curves, respectively. Fig. 4 (a) (top left panel) describes unstrained graphene in the external magnetic field. It corresponds to the situation studied experimentally in [5]. We observe that the positive (negative) energy states reside on A (B) sublattice. Since these states are associated with different valleys, the LLL is indeed valley polarized. Furthermore, the sublattice asymmetry is also seen for higher levels, because we took a large value of the gap $\Delta = 50$ meV. Fig. 4 (b) (top right panel) describes strained graphene in zero magnetic field. As it should be, the LLL is indeed completely sublattice polarized, while higher levels are polarized in the same fashion as in Fig. 4 (a). The PMF dominated regime, $|eB| < |B_{\rm pm}|$, is shown in Fig. 4 (c) (bottom left panel). The LLL polarization is similar with Fig. 4 (b). The magnetic field dominated regime, $|eB| > |B_{\rm pm}|$, is shown in Fig. 4 (d) (bottom right panel) and it is similar to Fig. 4 (a). Fig. 4 (c) and (d) are computed for the same values of the parameters as Fig. 1 (a) and (b), respectively. When both fields are present the asymmetry between the sublattices can be enhanced even for higher levels.

We note that in the present work the sublattice asymmetry is directly brought by the inversion symmetry gap Δ. We established that the presence of PMF and

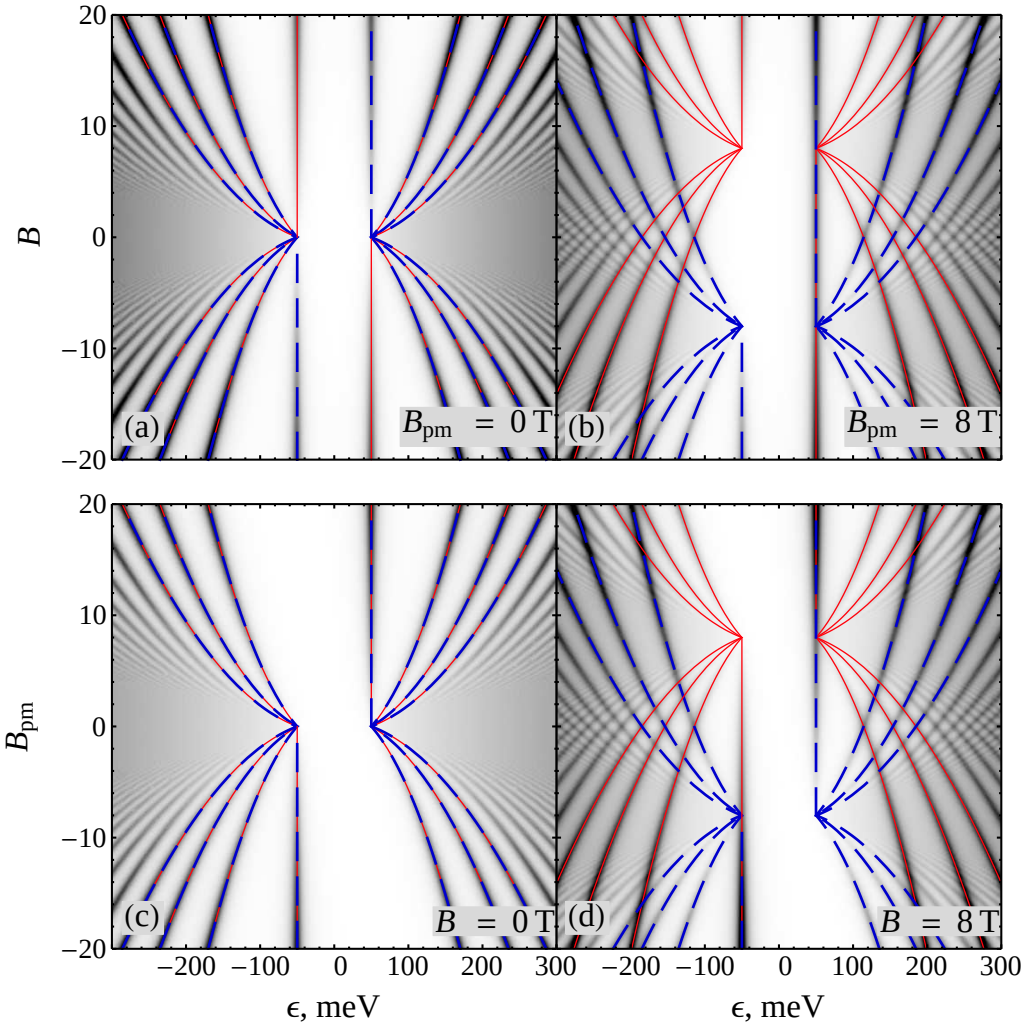

Figure 3. Density map of the full DOS $D(\epsilon, B, B_{\rm pm})$ as a function of energy ϵ in meV, magnetic field B in T and PMF in T. Top left panel: (a): for a constant $B_{\rm pm} = 0$ T. Top right panel: (b): for a constant $B_{\rm pm} = 8$ T. Bottom left panel: (c): for a constant $B = 0$ T. Bottom right panel: (d): for a constant $B = 8$ T. The density-map is overlaid with red and blue curves that show the position of the peaks originating from $\mathbf{K}$ and $\mathbf{K}'$ points. The gap $\Delta = 50$ meV, the scattering rate $\Gamma = 5$ meV and the Landau scale $\epsilon_0 = (\hbar v_F^2 B_\pm)^{1/2} = 25.7\sqrt{B_\pm[\mathrm{T}]}$ meV in all cases.

magnetic field further enhances this effect. It is shown in [29] that the local sublattice

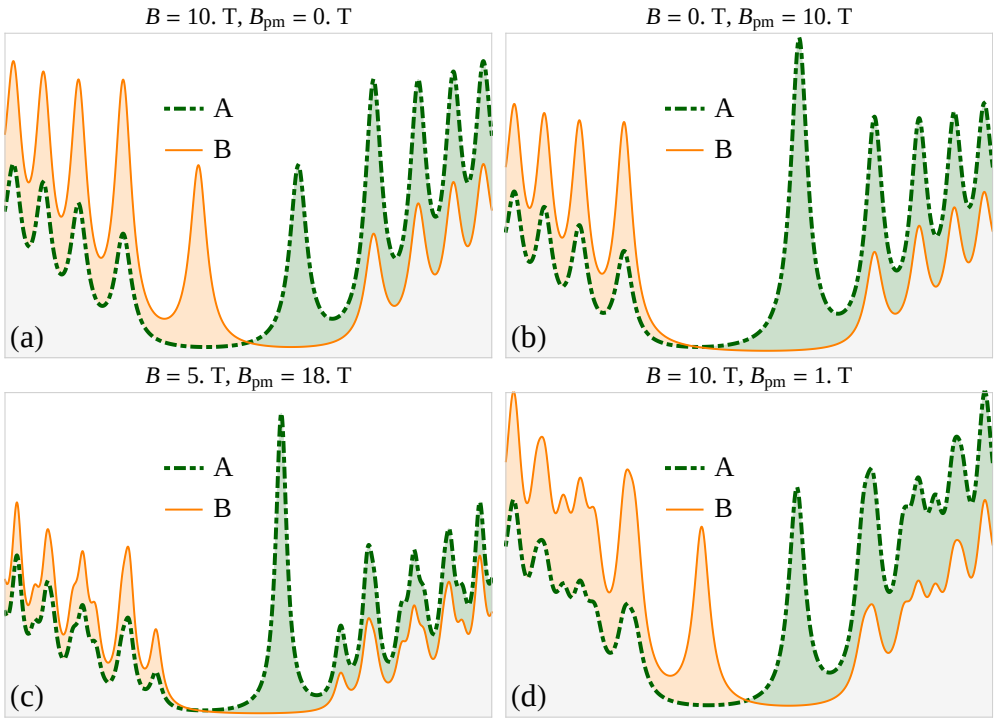

Figure 4. (Colour online) The sublattice resolved DOS, $D_A(\epsilon)$ (dashed) and $D_A(\epsilon)$ (solid) in arbitrary units as the functions of energy ϵ/ϵ_0. Top left panel: (a): in the absence of PMF, $B_{\rm pm} = 0$ and $B = 10$ T. Top right panel: (b): in the absence of magnetic $B = 0$ T, $B_{\rm pm} = 10$ T. Bottom left panel: (c): the fields $B = 5$ T and $B_{\rm pm} = 18$ T. Bottom left panel: (d) the fields $B = 10$ T and $B_{\rm pm} = 1$ T. The gap $\Delta = 50$ meV and the scattering rate $\Gamma = 10$ meV in all cases.

symmetry can be broken just by the deformation. This deformation is not a pure shear, so it produces not only the PMF, but also a scalar potential.

6. Conclusion

In the present work we had in mind that the sublattice resolved DOS can be measured by STS. However, the full DOS can also be experimentally found by measuring the quantum capacitance [27] which is proportional to the thermally smeared DOS. The corresponding convolution with a Fermi distribution is easily expressed in terms of the digamma function [30], so that the presented here results can be easily applied for this case.

In conclusion we note, that controlling the valley degree of freedom is important for possible valleytronics applications of the new materials. In this respect a simultaneous tuning of the strain (PMF) and magnetic field is rather useful, because it allows to remove the valley degeneracy. Thus the experimental testing of the features discussed in this work would be helpful for development of valleytronics.

Acknowledgments

We gratefully acknowledge E.V. Gorbar, V.P. Gusynin and V.M. Loktev for helpful discussions. S.G.Sh. acknowledges the support of EC for the RISE Project CoExAN GA644076.

References

[1] Mecklenburg M and Regan B C 2011 *Phys. Rev. Lett.* **106** 116803
[2] Castro Neto A H, Guinea F, Peres N M R, Novoselov K S and Geim A K 2009 *Rev. Mod. Phys.* **81** 109
[3] Goerbig M O 2011 *Rev. Mod. Phys.* **83** 1193
[4] Andrei E Y, Li G and Du X 2012 *Rep. Prog. Phys.* **75** 056501
[5] Wang W-X, Yin L-J, Qiao J-B, Cai T, Li S-Y, Dou R-F, Nie J-C, Wu X and He L 2015 *Phys. Rev. B* **92** 165420
[6] Gusynin V P, Sharapov S G and Carbotte J P 2007 *Int. J. Mod. Phys. B* **21** 4611
[7] Settness M, Power S R and Jauho A-P 2016 *Phys. Rev. B* **93** 035456
[8] Vozmediano M A H, Katsnelson M I and Guinea F 2010 *Physics Reports* **496** 109
[9] Amorim B, Cortijo A, de Juan F, Grushin A G, Guinea F, Gutierrez-Rubio A, Ochoa H, Parente V, Roldann R, San-Jose P, Schiefele J, Sturla M and Vozmediano M A H 2016 *Phys. Rep.* **617** 1
[10] Roy B and Herbut I F 2011 *Phys. Rev. B* **83** 195422
[11] Guinea F, Katsnelson M I and Geim A K 2010 *Nat. Phys.* **6** 30
[12] Levy N, Burke S A, Meaker K L, Panlasigui M, Zettl A, Guinea F, and Catro Neto A H and Crommie M F 2010 *Science* **329** 544
[13] Klimov N N, Jung S, Zhu S, Li T, Wright C A, Solares S D, Newell D B, Zhitenev N B and Stroscio J A 2012 *Science* **336** 1557
[14] Downs C S C, Usher A and Martin J 2016 *J. Appl. Phys.* **119** 194305
[15] Zhu S, Stroscio J A and Li T 2015 *Phys. Rev. Lett.* **115** 245501
[16] Roy B, Hu Z-X and Yang K 2013 *Phys. Rev. B* **87** 121408R
[17] Suzuura H and Tsuneya T 2002 *Phys. Rev. B* **65** 235412
[18] Ramezani Masir M, Moldovan D and Peeters F M 2013 *Solid State Commun.* **175-176** 76
[19] Kim K-J, Blanter Ya M and Ahn K-H 2011 *Phys. Rev. B* **84** 081401R
[20] Chodos A, Everding K and Owen D A 1990 *Phys. Rev. D* **42** 2881
[21] Gusynin VP, Miransky V A and Shovkovy I A 1994 *Phys. Rev. Lett.* **73**, 3499 ; 1995 *Phys. Rev. D* **52** 4718
[22] Sharapov S G, Gusynin V P and Beck H 2003 *Phys. Rev. B* **67** 144509
[23] Miransky V A and Shovkovy I A 2015 *Phys. Rep.* **576** 1
[24] Rybalka D O, Gorbar E V and Gusynin V P 2015 *Phys. Rev. B* **91** 115132
[25] Gradshteyn I S and Ryzhik I M 1980 Table of Integrals, Series and Products (Moscow: Nauka 1971; New York, Academic)
[26] Sharapov S G, Gusynin V P and Beck H 2004 *Phys. Rev. B* **69** 075104
[27] Ponomarenko L A, Yang R, Gorbachev R V, Blake P, Mayorov A S, Novoselov K S, Katsnelson M I and Geim A K 2010 *Phys. Rev. Lett.* **105** 136801
[28] Gorbachev R V, Song J C W, Yu G L, Kretinin A V, Withers F, Cao Y, Mishchenko A, Grigorieva I V, Novoselov K S, Levitov L S and Geim A K 2014 *Science* **346** 448
[29] Schneider M, Faria D, Viola Kusminskiy S and Sandler N 2015 *Phys. Rev. B* **91** R161407
[30] Gusynin V P, Loktev V M, Lukyanchuk I A, Sharapov S G and Varlamov A A 2014 *Fiz. Nizk. Temp.* **40** 355 [Engl. trans.: 2014 *Low Temp. Phys.* **40** 270]